Journal of Catalysis 292 (2012) 64–72

Contents lists available at SciVerse ScienceDirect

Journal of Catalysis

journal homepage: www.elsevier.com/locate/jcat

Hydrogenation of benzene and toluene over size controlled Pt/SBA-15 catalysts: Elucidation of the Pt particle size effect on reaction kinetics

Vladimir V. Pushkarev [a], Kwangjin An [a], Selim Alayoglu [b], Simon K. Beaumont [b], Gabor A. Somorjai [a,b,c,*]

[a] University of California Berkeley, Department of Chemistry, D54 Hildebrand Hall, Berkeley, CA 94720, USA
[b] Materials Sciences Division, Lawrence Berkeley National Laboratory, 1 Cyclotron Rd., Berkeley, CA 94720, USA
[c] Chemical Sciences Division, Lawrence Berkeley National Laboratory, 1 Cyclotron Rd., Berkeley, CA 94720, USA

ARTICLE INFO

Article history:
Received 8 December 2011
Revised 26 April 2012
Accepted 28 April 2012
Available online 4 June 2012

Keywords:
Benzene hydrogenation
Pt nanoparticles
Structural sensitivity
Compensation effect

ABSTRACT

Vapor-phase hydrogenation of benzene and toluene over a size-dependent (1.5–5.2 nm) series of Pt nanoparticles (NPs) encapsulated in polyvinylpyrrolidone (PVP) or polyamidoamine (PAMAM) dendrimer and supported in SBA-15 mesoporous silica was investigated at ambient pressure between 343 K and 398 K. Under these conditions, both reactions exhibit a moderate structure sensitivity evidenced by changes in their turnover rate (TOR), apparent activation energy (E_A), pre-exponential factor $\ln(r_0)$, and deactivation rate parameters with Pt particle size. For instance, the 2.4–3.1 nm Pt NPs showed the highest TOR for both reactions as compared to NPs of either smaller or larger sizes. Also, the E_A and $\ln(r_0)$ factor values were larger for smaller Pt particle sizes, and the rates of catalyst deactivation were more pronounced for catalysts with larger Pt particle sizes. However, the reaction orders on H_2 and hydrocarbon were independent of particle size.

Published by Elsevier Inc.

1. Introduction and background

Achieving the highest possible performance in catalytic reaction processing is an essential goal of the chemical industry. In aiming to develop catalysts with by the highest product yields and process stability, we concentrate our effort on understanding at the molecular level how the active component's particle size and shape, elemental composition, interaction with the support, presence of a surface dopant, catalytic poison, or capping agent affect the catalytic performance in industrially significant reactions [1–3]. In order to achieve this goal, material synthesis techniques on the nanoscale become crucial. These techniques give unique access to catalytic structures with a high degree of control of their essential properties. These structures can then be employed to isolate and study the influence of the various factors that determine catalytic performance individually. Recent progress in colloidal synthesis of nanostructured materials has provided us with the tools to produce sub-ten nanometer (<10 nm) NPs of platinum, rhodium, palladium, and gold, and their bimetallic combinations, while at the same time controlling the particle's composition, morphology, and size [4–14]. By employing transition metal NPs of very uniform size, we have shown that the product selectivities of many multi-path heterogeneous catalytic reactions were particle size and shape dependent [2]. In this work, we turn to single product catalytic reactions in order to examine sensitivity to Pt particle size by using colloidal platinum NPs. In particular, the effect on a number of key kinetic reaction parameters is considered: turnover rates, activation energies, pre-exponential factors, reaction orders, and rates of deactivation. We report on vapor-phase hydrogenation of monoaromatic hydrocarbons, benzene, and toluene, under ambient pressure conditions in the 343–398 K temperature range. These reactions have been studied previously in great detail using traditional Pt catalysts with relatively broad size distributions and had been designated structure insensitive reactions [15–20]. However, in this work, by employing colloidal Pt NPs with narrow size distributions, it is possible to explore the effect of catalyst metal particles size for small <10 nm particles in a controlled manner. The standard deviation in the diameter of particles prepared in this manner is around 20% in the examples used for the present study (e.g., 1.5 ± 0.3 nm) – this is very different from those prepared using conventional technologies. Fig. S1 (supplement) shows an example of one such catalyst obtained from Sigma-Aldrich in which the size distribution is 2.6 ± 2.3 nm, which corresponds to ±88% of the mean particle size. A typical example of catalysts used for studying benzene hydrogenation's structure sensitivity is similar with the smaller particles having a distribution of around 1.6 ± 1.4 nm (or ±85%) [16]. While when early investigations of the structure sensitivity were being carried out, investigators did

* Corresponding author at: University of California Berkeley, Department of Chemistry, D54 Hildebrand Hall, Berkeley, CA 94720, USA. Fax: +1 510 643 9668.
E-mail address: somorjai@berkeley.edu (G.A. Somorjai).

0021-9517/$ - see front matter Published by Elsevier Inc.
http://dx.doi.org/10.1016/j.jcat.2012.04.022

a commendable job we now have access to materials with a much narrower size distribution and can thus investigate this topic with much greater sensitivity.

In 1969, Boudart introduced a classification of heterogeneous catalytic reactions as being either structure sensitive or structure insensitive [15]. At the root of this distinction was experimental evidence that for some catalytic reactions, the specific reaction rates depended on the particle size distribution of the active metal, while for others there was no such dependence. Boudart's explanation for the existence of such structural sensitivity was based on Kobosev's *active ensemble* (geometric) theory that for catalyst particles within a certain size range (1–5 nm) the surface structure of a metal crystallite is expected to change. This arises as certain configurations or 'ensembles' of atoms may occur with varying frequencies depending on the crystallite size. If the rate of a chemical reaction depends on the availability of catalyst sites with a particular configuration, such reaction is expected to exhibit changes in specific reaction rate with particle size – said to be structure sensitive. If the reaction occurs such that it does not depend on specific arrangements of surface atoms – for instance occurring at a single metal atom – the reaction is structure insensitive.

The criterion Boudart used to discriminate between these two reaction types was whether the specific reaction rate varied with a factor of 10 over changing particle size distributions. Given the broad distributions of particle sizes in typical catalysts used in these types of studies, exercising such caution was then appropriate. Since many surface sites do not vary dramatically with particle size, this classification essentially limits structure sensitivity to reactions that either require large planes of atoms or else require low coordination edge or corner sites. For instance, the fraction of surface sites in flat terrace sites only decreases by around 50% on going from 10 down to 2 nm (calculating assuming a spherical cubo-octohedral shape on the basis of the models proposed by Hardeveld and Hartog [21] – examples of these sorts of calculation are given in the Supporting information). This means that truly structure-sensitive reactions may be manifested in specific activity changes that are actually much smaller than those different by a factor of 10. Today, we have uniform-sized metal nanoparticles, which can be fine tuned in size much more controllably than in previous decades – here, we exploit this to look for the sensitivities of specific reaction rates to particle size that were previously difficult to discriminate.

In order to adopt colloidally prepared nanoparticles as catalysts, we have in recent years carefully characterized many aspects of these systems – a key question being the effect of residual 'capping agent' material upon catalytic activity. These capping agents are used to control nanoparticle growth and give rise to the narrow size distributions obtained; however, despite extensive washing, some such material inevitably remains upon the nanoparticles following the colloidal synthesis. We and others have explored whether particles of the same size and shape prepared with different capping agents have similar available metal surface area and catalytic behavior. Specific cases of using organic capping agents to deliberately tailor the reactivity of a catalyst have been reported, such as the use of phenanthrolenes in regioselective hydrogenations [22]. However, very similar results were obtained both between PVP and oleylamine for C_2H_4 hydrogenation [23] and between PAMAM dendrimer and PVP-derived Pt catalysts [24]. Others also reported that for ~5 nm particles used in both 2-butyne-1,4-diol and styrene oxide hydrogenations, the differences in activity and selectivity were minimal for catalysts derived from nanoparticles prepared using PVA, PVP, or poly(methylvinylether) capping agents [25]. One interesting assessment of the impact of capping agent was made by treating a World Gold Council reference catalyst with PVP in the oxidation of benzyl alcohol – the study showed even washing could recover activity to at least 50% of the original reference catalyst [26]. It appears therefore that since these commonly used capping agents, which are quite different from one another, can be varied without perturbing the chemistry occurring, there is a minimal effect on the actual reactions. To quantify the residual capping agent after catalyst pre-treatment, 1.7–7.1 nm Pt/PVP nanoparticle catalysts were studied using H_2 chemisorption – the availability of surface sites was found to be reduced from that predicted from TEM, but by a consistent fraction as a function of particle size [27]. The catalyst pre-treatment was also investigated spectroscopically: both the degradation of the capping agent [28] and formation of a polyene-polyamide residue was observed after catalyst pre-treatments above 200 °C (as also used in this study) [29]. The Pt NPs are deposited within the channels of a SBA-15, a model low acidity mesoporous silica support selected to provide high surface area to ensure the stability of the catalyst without agglomeration that may otherwise result during deposition. The low acidity also minimizes the interference of H_2 spillover effects in the reliable measurement of catalyst activities [30]. The supported nanoparticles after deposition in the channels of the SBA-15 mesoporous SiO_2 are shown in Fig. 2S. The strong interaction of the particles and support is indicated by the fact that they remain in the support despite multiple washing in ethanol (an otherwise dispersive solvent for the nanoparticles). Additionally, no stray unsupported particles are seen in the TEM, which was prepared by drop casting a sample of the supported catalyst sonicated in ethanol.

Having carefully characterized the system in this way, we can now truly explore the size effect for small, sub-ten nanometer particles in a controlled manner. It has already been demonstrated by this method that the Heck reaction appears to exhibit this sort of mild structure sensitivity behavior in this regime using Pd/PVP nanoparticles, and the activity found to correlate very well with the presence of defect sites [31].

Benzene/toluene hydrogenations are reactions relevant to both the petrochemical and fine chemical industries. Despite the fact that the benzene ring hydrogenation over Pt is one of the most studied catalytic reactions, neither the true role of the support, nor the reaction mechanism on the Pt surface itself has been unambiguously determined. Studies dating back up to four decades have produced contradictory results – some indicating that benzene hydrogenation over supported Pt catalysts is structure insensitive [15–20], while others claim it to be structure sensitive [32]. Recent studies of this reaction by a combination of reaction kinetics and *in situ* sum-frequency generation (SFG) vibrational spectroscopy on single crystal surfaces of Pt and on uniform-sized, shape-controlled Pt nanoparticles have revealed that benzene hydrogenation can be structure sensitive [33–35]. Indeed, benzene hydrogenation over a Pt(111) single crystal surface results in the formation of two reaction products: cyclohexane and cyclohexene [33]. On Pt(100), however, only a single reaction product, cyclohexane, is observed [34]. This is consistent with the kinetics measured over Pt nanoparticles with controlled shapes. For instance, Bratlie et al. reported the formation of both cyclohexene and cyclohexane reaction products on Pt nanocrystals with cubeoctahedral shapes that are predominantly terminated with {111} facets [35]. On the other hand, under similar reaction conditions for the Pt nanoparticles with cubic shapes, which are predominantly terminated with {100} facets, only cyclohexane reaction product could be detected.

Here, we find that vapor-phase hydrogenation of both benzene and toluene over Pt is, in fact, structure sensitive in this sub-ten nanometer regime. This and similar studies that employ size-controlled transition metal NPs as model catalysts serve to highlight the importance of being able to precisely control the active component's size, shape, and composition, as well as interactions with the

support, in order to achieve optimal catalytic performance. In addition, it also becomes clear that superior catalytic activity may be obtained by using certain sizes of transition metal NPs. Coupled with their generally good resistance to deactivation and the size/shape dependence of selectivity in many multipath reactions, we believe that there are compelling reasons for the use of size-controlled metal nanoparticles to improve upon the traditional metal catalytic systems with broad size distributions in both catalysis science and in industrial chemical processing.

2. Experimental part

2.1. Materials

The $H_2PtCl_6{\cdot}6H_2O$ and K_2PtCl_4 (both 99.9% pure on metals basis), PVP (Mw = 55,000 g/mol), Pluronic P123 (M_n = 5800, EO_{20}-$PO_{70}EO_{20}$, EO = ethylene oxide, PO = propylene oxide), and tetraethoxysilane (TEOS, 98%) were purchased from Sigma-Aldrich. The fourth-generation –OH-terminated PAMAM dendrimer (Mw = 14215 g/mol) as a 10.2 wt.% in methanol solution was purchased from Dendritech. The liquid hydrocarbons: pentane, benzene, and toluene were used without further purification (all anhydrous, 99.9%, Sigma-Aldrich). The H_2 and N_2 gases (high purity, >99.995%, PraxAir) used in reaction studies were additionally purified by passing through oxygen scrubber traps (Supelpure, Supelco).

2.2. Material synthesis

The general synthetic approach for the preparation of the 1.5–5 nm sizes of Pt NPs capped with polyvinylpyrrolidone (PVP) was previously described in the literature [8,9], and the specific details are provided in the Supporting information, as is the synthetic method for the preparation of the 2.4 nm Pt-dendrimer NPs. SBA-15 mesoporous silica was synthesized according to the method reported in the literature [36] and described in the Supporting information.

The SBA-15-supported catalysts were prepared by mixing the mesoporous silica powder with colloidal solutions of Pt NPs in ethanol, then subjecting the mixture to sonication for 3 h at room temperature in a commercial ultrasonic cleaner (1510R-MT, 70 W, Branson). After immobilization of the NPs in the support, the resulting precipitate was separated by centrifugation (3000 rpm, 20 min). (The samples prepared using PVP were thoroughly washed with ethanol to ensure removal of excess polymer at this stage.) The resulting catalysts were dried in air at 373 K overnight before use.

2.3. Material characterization

The sizes of the Pt NPs were analyzed using a Hitachi H-7650 transmission electron microscope (TEM) operated at 120 kV. High resolution (HR) and annular dark field (ADF) TEM pictures were obtained using a Jeol 2100 LaB_6 microscope and a Jeol 2100-F microscope, both operating at 200 kV, respectively. The average TEM-projected Pt particle sizes and the size distribution histograms were typically determined from TEM images by counting 200–300 particles. Fig. 1 shows the particle size distribution histograms, the mean sizes and standard deviations of the size-dependent series of Pt NPs. HRTEM pictures (Fig. S3) indicate nanocrystalline Pt nanoparticles with polyhedral shapes (i.e., spherical). TEM pictures of the spent catalysts of Pt nanoparticles supported in mesoporous silica (Fig. S2) show negligible particle sintering or morphological changes. X-ray diffraction (XRD) patterns were obtained using a Bruker D8 diffractometer with a Co source and general area 2-dimensional detector system (GADDS). XRD patterns in Fig. S4 show nanocrystalline Pt phase with (111), (200) and (220) reflections broadening gradually with decreasing particle sizes from 5 nm to 1.5 nm, as predicted by the Debye equation [37]. The total Pt loadings were determined by inductively coupled plasma atomic emission spectroscopy (ICP-AES) using a Perkin Elmer optical emission spectrometer (Optima 7000 DV). The instrument was calibrated using a platinum standard (Fluka, TraceCERT 1000 mg/l). The total specific surface area of SBA-15 support and catalyst samples was determined via N_2 (UHP grade, 99.999%, PraxAir) physisorption at 77 K using an Autosorb-1 (Quantachrome) analyzer.

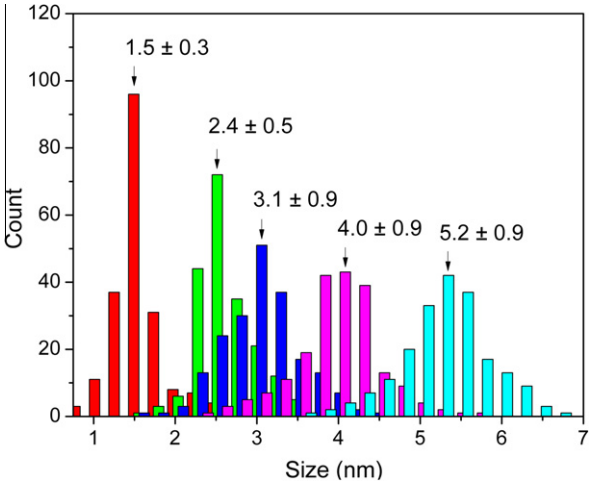

Fig. 1. Particle size distribution histograms of the Pt/SBA-15 series catalysts obtained from TEM images. The number inserts indicate the mean particle diameter and standard deviation for each sample.

2.4. Kinetics measurements

Reaction kinetic measurements of benzene and toluene hydrogenation were conducted in the vapor phase in a plug-flow fixed catalyst bed microreactor test system, which was built around a single vertically mounted stainless steel tubular (55 cm long, 0.6 cm O.D., 0.45 cm I.D.) reactor positioned inside of a tubular furnace (Model 3210, Applied Test Systems). The H_2 and N_2 gas flow rates were controlled with Brooks mass flow controllers (5850E type) in the 2–100 sccm range for each gas. The reactor inlet pressure was monitored using a capacitance manometer transducer (Baratron 890B, MKS Instruments). The reactor outlet was connected to a hydrocarbon scrubber, which was connected to the vent, and the reactor outlet pressure was assumed to be 101.35 kPa. The quantitative analysis of reactants and reaction products was done chromatographically using a Hewlett–Packard (5890 Series II) gas chromatograph equipped with a 10 m dimethylpolysiloxane (HP-1, Hewlett–Packard) capillary column, a computer interface and Chemstation data acquisition and processing software (Agilent).

Prior to loading into the reactor, each catalyst sample was pelletized by compressing the material powder in a punch/die set using a hydraulic press at 400 kg/cm^2 for 3 min, then by crushing, sieving and collecting the 0.7–0.45-mm granules. The resulting granulate was loaded into the stainless steel reactor, forming the catalyst bed. The amount of catalyst used in a single experiment was 0.150 g, and the catalyst bed height was 4 cm. Geometrically, the catalyst bed was positioned in the middle of the reactor height, limited by small amounts of purified glass wool at each end. The remaining inner volume of the reactor was filled

with a purified (etched in concentrated HCl,[1] washed with deionized water and calcined at 923 K in air) alundum (α-Al_2O_3, Henan Sicheng) with 0.7–0.45-mm granules. The catalyst pre-treatment consisted of a reduction in a flow of a 50 vol.% mixture of H_2 and N_2 at 20 sccm total flow rate. The reduction treatment was performed under ambient pressure at 533 K for 2 h. The heating/cooling rate during catalyst reduction treatment was 1 K/min. All catalytic measurements were taken on multiple samples of any given catalyst material.

Prior to the measurements, an aromatic hydrocarbon (benzene or toluene) was dissolved in an excess of liquid *n*-pentane, forming a hydrocarbon:*n*-pentane = 1:4 volume ratio solution (at 293 K). First, the hydrocarbon solution was degassed by bubbling Ar gas through it for 30 min. Then, the solution was fed at 1.0–2.0 cc/h flow rate using a syringe pump (Kent Scientific) equipped with a Hamilton syringe (Gastight) into the preheating reactor header, which was maintained at 383 K. In the preheating zone, the hydrocarbon evaporated and the vapor was mixed with the flowing H_2 in N_2 gases, resulting in a four-component gas flow entering the reactor at near atmospheric pressure and the total flow rate ranging from 15 to 30 sccm. A 20-min delay period was allowed prior to taking a measurement for the system to equilibrate. At any time when experimental conditions were changed between the measurements, the hydrocarbon flow was cut-off and only H_2/N_2 flow was allowed to pass through the reactor so as to minimize catalyst deactivation. A 'fresh' catalyst was conditioned first under a stream of reactants at 363 K for 4 h. The purpose of this step was to allow for the adjustment of the catalyst to the presence of reactants and to achieve a pseudo steady-state catalytic performance under the reaction conditions. During this step, some catalysts indicated a deactivation behavior, but the loss of activity was less than 5% for any sample tested. Significant further deactivation was not observed during the acquisition of rate measurements. (At higher temperatures than those used in the rate measurements, some deactivation occurred as shown in Fig. 8.) Arrhenius dependence measurements were taken as an increasing temperature sequence. At each temperature point, the catalyst was held for 1.5 h in order to detect any deactivation during the measurement. The activity and partial pressure dependence measurements were taken at 363 K, while the Arrhenius dependence was measured between 343 and 398 K. During the measurements, the typical conversions were below 5%, while the maximum conversion (at 398 K) did not exceed 15%. The analysis of kinetics data following the model developed by Post et al. revealed that mass transfer limitations under these experimental conditions were negligible [38]. Further confirmation was provided that the rate measurements were recorded in the absence of diffusion control or thermal gradients by using the Madon–Boudart criterion as described in the Supporting information (Fig. S5) [39]. The ethylene hydrogenation activities were determined using the setup and under reaction conditions that have been described elsewhere, using the known TOR of 10 molecules of ethylene (surface Pt atom)$^{-1}$ s^{-1} at 293 K, 100 torr H_2, and 10 torr C_2H_4 [24,40].

3. Results

The effect of temperature on turnover frequencies in the vapor-phase hydrogenation of benzene and toluene over the size-dependent series of Pt/SBA-15 catalysts is shown by the Arrhenius plots in Fig. 2a and b, respectively. The measurements were taken in the 343–398 K temperature range using reaction mixture flows

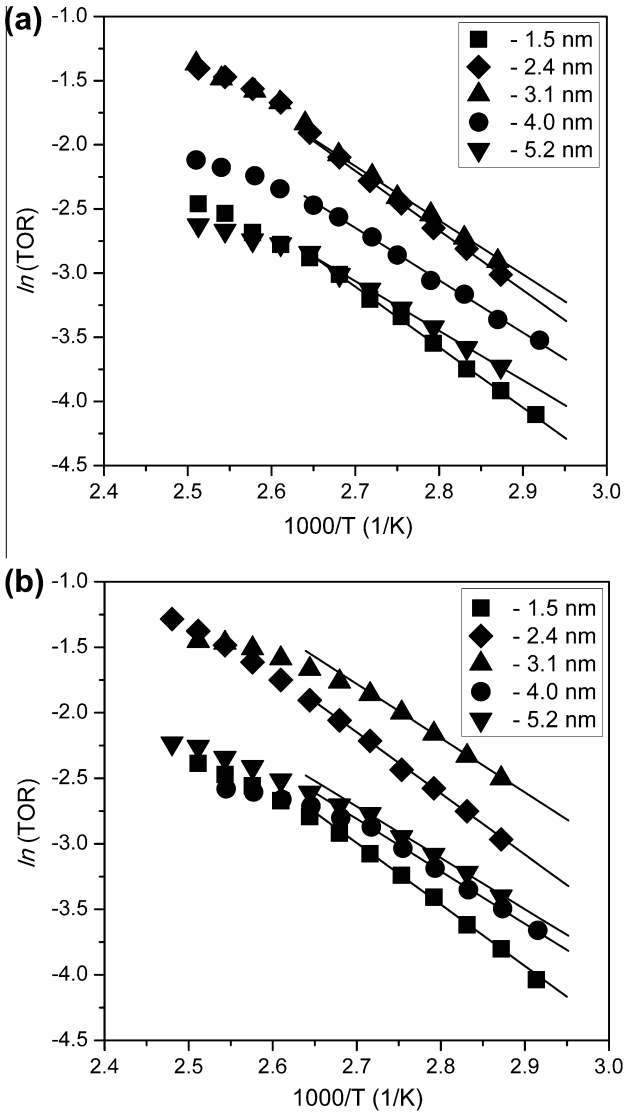

Fig. 2. Arrhenius pots for (a) benzene hydrogenation under 6.40 kPa benzene and 23.20 kPa H_2 and (b) toluene hydrogenation under 5.33 kPa toluene and 23.47 kPa H_2, both measured in the 343–398 K temperature range. Catalytic activity is expressed as a TOR numbers, [molecules Pt site^{-1} s^{-1}], for the formation of cyclohexane or methylcyclohexane product from benzene or toluene hydrogenation, respectively.

containing 6.40 kPa benzene and 23.20 kPa H_2 for benzene hydrogenation and 5.33 kPa toluene and 23.47 kPa H_2 for toluene hydrogenation. Under these conditions, the only detectable reaction products were cyclohexane for benzene hydrogenation and methylcyclohexane for toluene hydrogenation. The Arrhenius plot dependencies for both reactions were linear with temperature between 343 and 368 K Fig. 2a and b, while above 368 K the ln(TOR) values progressively deviated below the linear regression line on the Arrhenius plot with increasing temperature. This type of behavior has been widely reported for both reactions and is attributed to both a decrease in the surface coverage of the reactant or intermediates that occurs at temperatures above 368 K and a thermodynamic limit resulting from the reactions exothermic nature making the forward reaction less favorable at higher temperatures and producing an equilibrium between benzene–hydrogen–cyclohexane, although calculation of the equilibrium with temperature indicates this is more likely above 500 K as indicated in the Supporting information (Fig. S7). This effect was reported in considering benzene hydrogenation over Ni [41]. The lower surface coverage

[1] It should be noted that although residual chlorine could potentially migrate and effect the activity of the catalyst, it has been reported for arene hydrogenation that chlorine has no effect on the reaction [16].

of the reactant or favoring of the forward reaction, in turn, negatively impacting on the measured reaction rates [33,34,42]. Also, some have suggested that the effect could be due to the loss of catalytically active sites to surface carbon poisoning as a result of cracking of the reactants during the experiment could be responsible for the effect [43]. In this work, at temperatures below 373 K, the measured loss of activity for any of the catalysts studied was under 1% h^{-1} and the evaluation of all reaction kinetics parameters was performed below this temperature.

The E_A and $\ln(r_0)$ factor values determined from the linear Arrhenius regressions in the 343–368 K temperature range for benzene and toluene hydrogenation reactions are plotted against the mean Pt particle size in Fig. 3a and b, respectively. In addition, the E_A and $\ln(r_0)$ factor values for both reactions are compared in Table S1. It should be noted that this assumes the partial pressure of H_2 is constant, since (as will be seen) the reaction is not zero order in H_2. Since the reaction typically proceeds only up to 5% (max. 15%) conversion and the concentration drop is on average half of this value (hydrogen is in a slight excess anyway), this assumption is reasonable within the experimental errors of our data. Fig. 4 is a Constable plot of $\ln(r_0)$ factor values against corresponding E_A values. From the data presented, it is evident that both E_A and $\ln(r_0)$ factor parameters correlate with mean Pt particle size and also show a mutual compensatory-type behavior. For instance, as shown in Table S1, the E_A values in benzene hydrogenation decreased from 39.0 ± 1.3 kJ/mol for 1.5 nm Pt to 32.3 ± 0.4 kJ/mol for 5.2 nm Pt, while the $\ln(r_0)$ factor values correspondingly decreased from 12.5 ± 0.5 to 8.1 ± 0.1 for the same particle sizes. Similarly, the E_A values in toluene hydrogenation decreased from 39.0 ± 0.8 kJ/mol for 1.5 nm Pt to 32.3 ± 1.3 kJ/mol for 5.2 nm Pt, while the $\ln(r_0)$ factor values decreased from 12.2 ± 0.2 to 8.3 ± 0.4.

The E_A values determined in this work were generally lower than the values reported in the literature for traditional supported Pt catalysts. For instance, Lin and Vannice reported E_A values in the range 42–55 kJ/mol for benzene hydrogenation [43] and 42–59 kJ/mol for toluene hydrogenation [44]. Flores et al. reported E_A values in the range 44–54 kJ/mol for benzene hydrogenation [32], while Basset et al. reported E_A values from 40 to 43 kJ/mol [16]. This difference can be attributed to the effect the capping agent has on the state of the Pt surface and also to a generally higher dispersion of Pt, and therefore smaller particle size, in the traditional supported catalysts. Indeed, the E_A value of 32.3 kJ/mol measured in benzene hydrogenation over the 5.2 nm Pt catalyst was identical to the values reported in the literature for unsupported Pt black powder [43] and also consistent with the values reported for a Pt(1 1 1) surface [34].

Fig. 5 shows the TOR values for benzene and toluene hydrogenation reactions measured at 363 K and plotted against the mean Pt particle size. The TOR values were calculated using the numbers of Pt sites available on the Pt/SBA-15 catalysts as determined from C_2H_4 hydrogenation turnover frequencies. Ethylene hydrogenation, a known structure-insensitive reaction, was used to probe the availability of surface sites, since this largely accounts for any site blocking or hindered access of the reactants to the catalyst due to residual capping agent left over from the synthesis. Ethylene

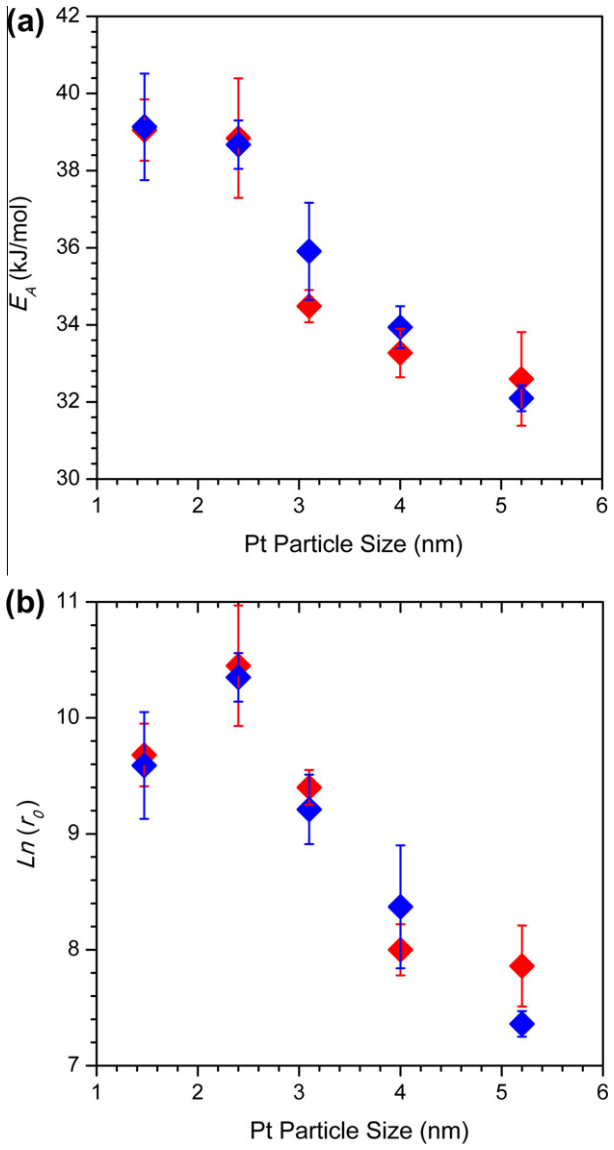

Fig. 3. (a) E_A and (b) $\ln(r_0)$ factor values plotted against mean Pt NPs size for benzene hydrogenation (blue symbols) and toluene hydrogenation (red symbols). The values were determined from the linear Arrhenius regressions (Fig. 2) in the 343–368 K temperature range. *Note*: the Arrhenius coordinate intercept, $\ln(r_o)$ is defined through the Arrhenius equation: $\ln(r) = \ln(r_o) - E_A/RT$. The error bars represent 95% confidence limits determined during the data fitting procedure. (For interpretation of the references to color in this figure legend, the reader is referred to the web version of this article.)

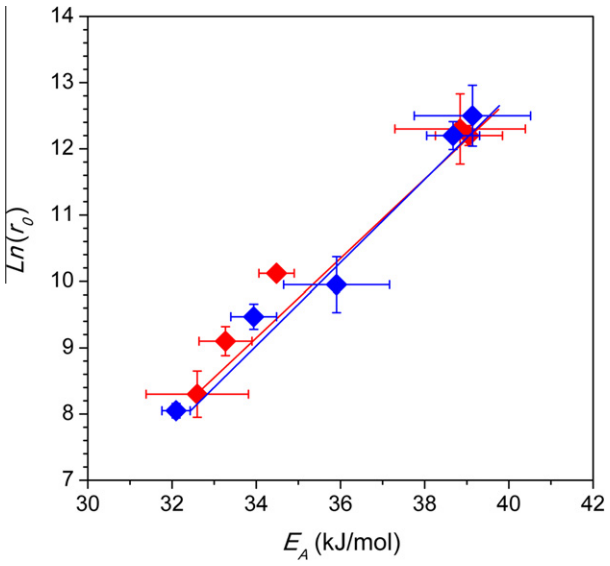

Fig. 4. Constable plots of $\ln(r_0)$ pre-exponential factor values plotted against the corresponding E_A values for benzene hydrogenation (blue symbols) and toluene hydrogenation (red symbols), the linear correlation showing a compensation effect. (For interpretation of the references to color in this figure legend, the reader is referred to the web version of this article.)

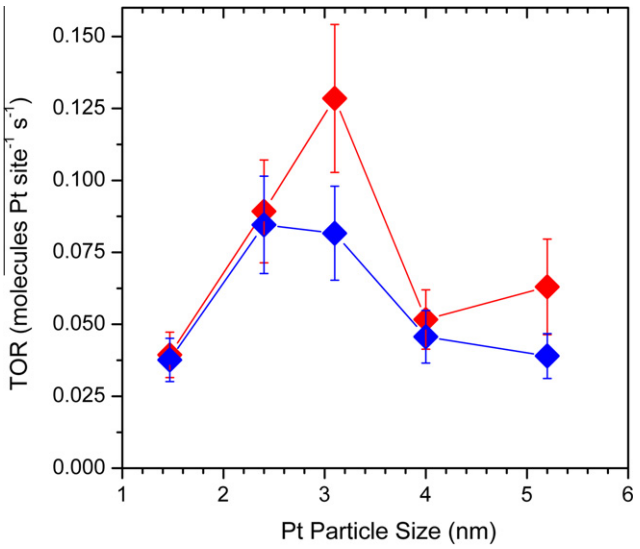

Fig. 5. TOR values (estimated by using the active site numbers determined from ethylene hydrogenation) for benzene hydrogenation (blue symbols) and toluene hydrogenation (red symbols) plotted against mean sizes of Pt NPs. The TOR dependencies were measured at 363 K using 6.40 kPa benzene and 23.20 kPa H_2 for benzene hydrogenation and 5.33 kPa toluene and 23.47 kPa H_2 for toluene hydrogenation. The C_2H_2 hydrogenation study was performed at 101.35 kPa of total pressure at 265 K in a 100 cc/min flow containing 2.67 kPa C_2H_4 and 16.0 kPa of H_2 with balance of He. (For the interpretation of the references to color in this figure legend, the reader is referred to the web version of this article.)

hydrogenation was selected as a low temperature structure sensitive probe reaction for calculating surface sites as reported previously by Kuhn et al. [23]. This method and other similar probe reactions (e.g., CO oxidation [45]) in our view provide a more useful measure of reactive surface sites for studying nanoparticle catalysts. These methods overcome the shortcomings of needing to use elevated temperatures that cause sintering and that the real catalyst may not necessarily be exposed to and eliminate errors due to H_2 spillover if H_2 chemisorption is used to titrate surface sites. In the case of capped Pt nanoparticles, we have previously compared H_2 chemisorption and ethylene hydrogenation as methods for determining the quantity of accessible surface metal atoms [23]. While a reliable estimate could sometimes be acquired from H_2 chemisorption, the values for samples treated at higher temperatures were vast overestimates of the reactive surface areas available. This resulted from H_2 spillover onto carbonaceous material.

Both the compensation effect pointing to the importance of reactant adsorption energies in the observed particle size effect and the consistent results obtained with a second quite different capping agent (2.4 nm particle, PAMAM dendrimer capping) serve to confirm the key effects observed cannot be primarily the result of residual capping agent. The TOR values between benzene and toluene hydrogenation were similar for the two smallest sizes of Pt NPs (1.5 nm and 2.4 nm), but differed for larger NP sizes. The TORs exhibited maxima at 2.4 nm Pt/SBA-15 for benzene hydrogenation (TOR of 0.084 ± 0.017 s^{-1}) and 3.1 nm Pt/SBA-15 for toluene hydrogenation (TOR of 0.128 ± 0.026 s^{-1}). These TOR values are within the range of 0.02–0.30 s^{-1} reported in the literature for these two reactions when measured under similar conditions [43,44] or extrapolated using E_A and reaction order in H_2 [16,46].

To investigate the effect of the Pt particle size on the reaction mechanism, the partial pressure dependencies on hydrogen and hydrocarbon were determined for both benzene and toluene hydrogenation across the size-dependent series of Pt/SBA-15 catalysts. A simple rate law for hydrocarbon hydrogenation expressed in a standard power law equation is assumed:

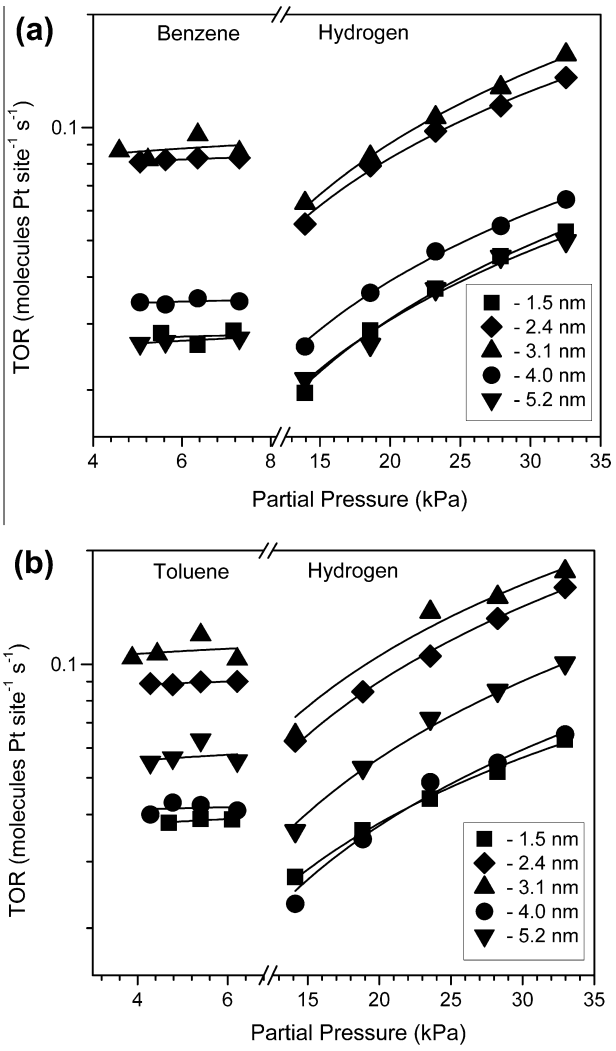

Fig. 6. Logarithm plots of the reaction rate over Pt/SBA-15 series catalysts in (a) benzene and (b) toluene hydrogenation at 363 K as a function of partial pressure of the hydrocarbon and hydrogen. (a) Benzene pressure dependence determined at 23.20 kPa H_2, while H_2 pressure dependence determined at 6.40 kPa benzene. (b) Toluene pressure dependence determined at 23.47 kPa H_2, while H_2 pressure dependence determined at 5.33 kPa toluene.

$$r = k p_{HC}^{\alpha} p_{H_2}^{\beta} \quad (1)$$

where r is the reaction rate, k is the reaction rate constant, p_{HC} and p_{H_2} are the partial pressures of hydrocarbon and hydrogen, respectively, and α and β are the reaction orders with respect to the hydrocarbon and hydrogen species. The reaction order determination for both reactions (see Fig. 6a and b) was performed at 363 K using similar partial pressure values for both reactants in order to be able to directly compare the results between benzene and toluene hydrogenation reactions measured in this work. The conditions were also selected to make comparisons with the values available from the literature feasible. Fig. 7 shows the reaction order values determined for hydrogen and hydrocarbon (benzene/toluene) and plotted as a function of mean Pt particle size. Both reactions have nearly identical reaction order dependencies: a slight positive reaction order in hydrocarbon and a value in the range of 1.0–1.2 for hydrogen. The reaction order values for hydrocarbon were consistent with the reported literature values: 0.1 ± 0.1 for benzene [43] and 0.1 ± 0.15 for toluene [44]. The reaction order of hydrogen was higher than the commonly reported 0.6 ± 0.1 value reported for benzene hydrogenation on Pt/Al_2O_3 [43], although the same

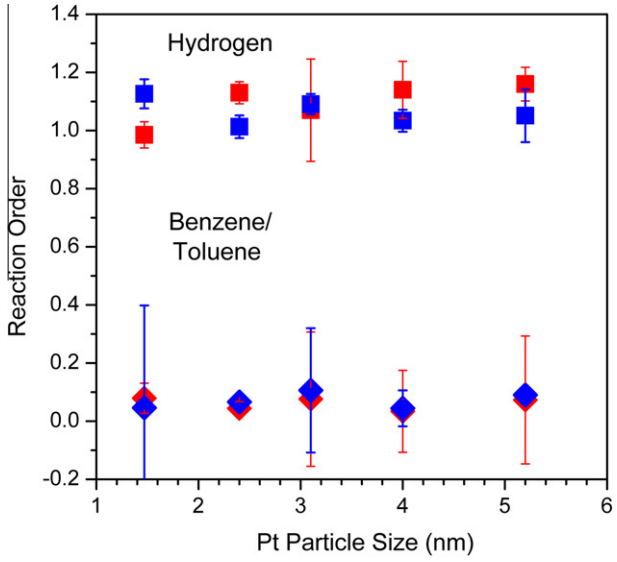

Fig. 7. Reaction order values for hydrogen (square symbols) and hydrocarbon (rhombic symbols) plotted against mean Pt NPs sizes for benzene (blue symbols) and toluene (red symbols) hydrogenation measured at 363 K. The error bars represent 95% confidence limits determined during the data fitting procedure. (For interpretation of the references to color in this figure legend, the reader is referred to the web version of this article.)

author notes that it has also been reported as unity in some case [43], but similar to 1.0 ± 0.2 values reported for toluene hydrogenation [44]. These reaction orders are reported to reflect a mechanism in which the rate-determining step is the addition of hydrogen to a surface intermediate that has already been formed from the arene [44]. Another noteworthy possibility is that the surface is crowded by hydrocarbon species and the chemisorption of hydrogen itself is a rate limiting or kinetically significant step. The reaction orders in H_2 and arene of both hydrogenations did not vary as a function of particle size, indicating no significant change in the hydrogenation reaction mechanism as a function of Pt particle size over the range studied (1.5–5.2 nm).

The benzene and toluene hydrogenation reactions on Pt surfaces are accompanied by side reactions in which the aromatic hydrocarbons dehydrogenate and polymerize blocking access to the active sites required for hydrogenation reaction pathways [43]. Fig. 8a and b summarize the measurements of the catalytic activity loss under steady reactant flow at 393 K for freshly reduced samples as a function mean Pt particle size. It should be noted this temperature is above that used in the determination of the other catalytic parameters as the formation of carbon species can better be compared under elevated temperature conditions where some degradation of activity occurs. Under typical conditions for the determination of other catalytic parameters, no more than 1% loss in activity per hour occurred and typically much less was observed. Fig. 8a shows the initial activity loss as a %-hourly rate, while Fig. 8b shows the cumulative loss of activity after 12 h time on stream. The polymeric surface carbon species, which form during reaction, can be removed in most cases and the initial activity restored by repeating the catalyst reduction treatment in hydrogen at 533 K. As it can be seen from Fig. 8a and b, the deactivation rate was particle size dependent with the smallest Pt size 1.5 nm showing very low initial and cumulative deactivation rates, while the larger Pt sizes deactivated faster. The 3.1 nm Pt/SBA-15 catalyst with the highest TOR in toluene hydrogenation also showed the fastest rate of deactivation. The rate of catalyst deactivation under benzene and toluene streams was generally similar for Pt NPs of any given size.

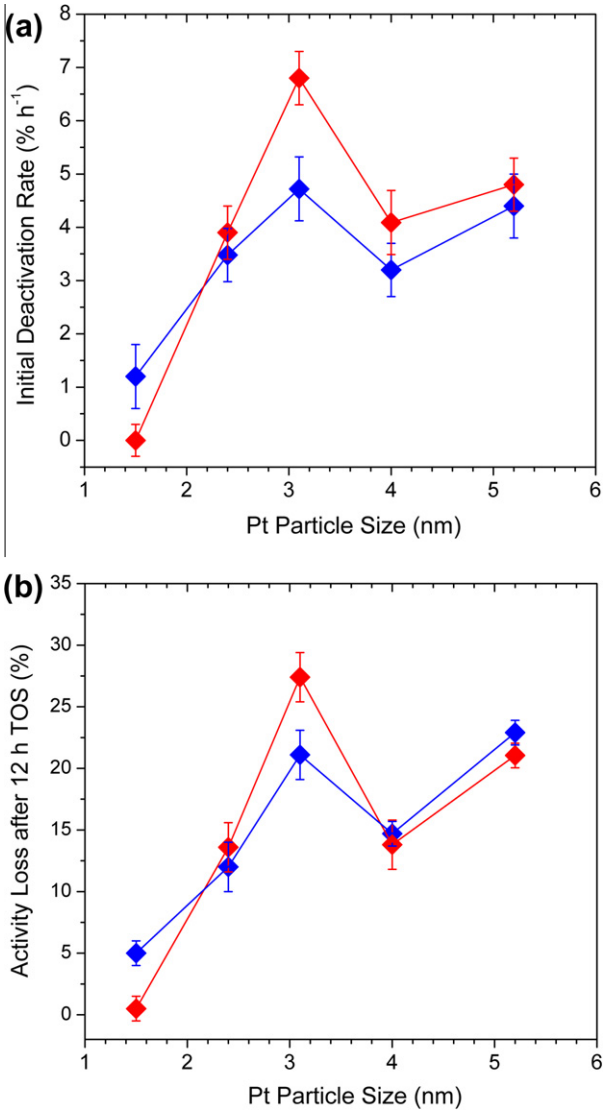

Fig. 8. Catalytic activity loss under a steady steam of reactants for hydrogenation of benzene (blue symbols) and toluene (red symbols) at 393 K showing a) initial % h^{-1} deactivation rate and b) cumulative loss after 12 h time on stream plotted against mean Pt NPs size. 23.20 kPa H_2 and 6.40 kPa of benzene were used in benzene hydrogenation and 23.47 kPa of H_2 5.33 kPa of toluene was used in the toluene hydrogenation reaction. (For the interpretation of the references to color in this figure legend, the reader is referred to the web version of this article.)

4. Discussion

Benzene hydrogenation over small Pt nanoparticles (1.5–5.2 nm) under the conditions studied follows the complete hydrogenation route with cyclohexane being the only detectable product. Nevertheless, the turnover rate measurements indicate a structural sensitivity that becomes pronounced for the Pt particle sizes in the range between 1.5 and 4 nm. The TOR change as a function of Pt particle size is less than a factor of three. It should be noted that the possibility of this 'structure sensitivity' originating in some way from the presence of the residual capping agent can be excluded as follows. The same capping agent, PVP, is used throughout, although as a further check, the reactivity was found not to differ when using a comparable sample prepared using PAMAM dendrimer. After treatment, there will be a fractional part of the surface with polyene-polyamide decomposition products of

PVP obstructing reactant access. It could also be suggested that such sites could act as sink for H_2 spillover. However, the fraction of obstructed sites does not change strongly with particle size such that it could cause the ~ 3-fold increase in TORs around 2–3 nm or correlate positively or negatively with the maximum in TOR.[2]

A compensation effect manifests itself as a correlation dependence between E_A and $\ln(r_0)$, shown in Fig. 4 and as can be seen from the values shown in Table S1. The compensation effect is known to exist for benzene hydrogenation over Pt surfaces [33]; however, this is the first instance for benzene hydrogenation in which it is shown for Pt particles of different sizes. Although at present, the confident ascribing of the compensation effect observed here to one or more causes still requires further work, some suggestions can be made as follows. Compensation effects of this type occur when the apparent activation energy determined experimentally is affected by other steps in the catalytic sequence. In heterogeneous catalysis when changing the catalyst rather than the reaction conditions such a compensation between the apparent (or experimentally determined) activation energy and the pre-exponential factor originates in changes of surface coverage [47]. This may in turn be determined by the adsorption coefficient (in Langmuir Hinshelwood type adsorption). In short, it most likely points to a change in the adsorption energy of the reactant or reactants. Since the observed structure sensitivity originates in the balance of E_A and $\ln(r_0)$, this may well also point toward the basis of the structure sensitivity suggesting that it is not the number of sites or different mechanistic pathways but instead due to the energy of adsorption of the reactants varying with particle size. This is highly plausible since, irrespective of particle shape, the availability of terrace atoms, edge atoms and corner atoms on the particles surface changes with shape (see example calculations provided in the Supplementary information) [21]. Since arenes interact with several atoms at a time (in contrast to the case of ethylene that coordinates to a single surface Pt atom so is truly structure insensitive), it is very likely indeed that the adsorption energy and therefore the surface coverages and energies of activation will vary with the adsorption site 'ensemble' and therefore with particle size. A further possible cause of such variations is the formation of dehydrogenated species being structure sensitive, which would affect the rate independently of E_A, as proposed by Lin and Vannice [43]. It is therefore possible that although reactive sites may undergo easier reactions (lower E_A), the relative surface coverages of the reactants are such that the overall reaction rate is still lowered.

5. Conclusion

Vapor-phase benzene and toluene hydrogenation reactions in the 343–393 K temperature range over uniformly sized Pt nanoparticles of different sizes were found to exhibit similar kinetic dependencies and are moderately structure sensitive based on changes to kinetic parameters upon changing the Pt particle size. Under these conditions, both reactions are highly selective toward complete hydrogenation of the aromatic ring, as no partial hydrogenation (e.g., cyclohexene/methylcyclohexane) products were detected. The Pt particle size variation has a marked effect on the E_A and $\ln(r_0)$ pre-exponential factor values. However, the contribution of these variations with particle size into the overall rate was diminished by a mutual compensation effect. The independence of the reaction orders of hydrogen and hydrocarbon on Pt particle size indicates the structural insensitivity of the principle reaction mechanism; this suggests other particle size-dependant factors, most likely reactant adsorption energy changes, cause the observed variation with particle size. The rate of catalyst deactivation due to the formation of hydrogen-deficient surface species was more pronounced for catalysts with larger Pt particle sizes, with 1.5 nm Pt NPs being highly resistant to deactivation.

[2] While one could speculate that the residual polyene-polyamide material could adsorb preferentially at certain sites, this would have no effect unless the arene hydrogenation was indeed surface sensitive and also seems unlikely in view of the fact the distribution of a polymer-like material is more likely to be controlled by the restrictions imposed by the polymer carbon chain and other adsorbates present.

Acknowledgments

This work is funded by the Office of Science, Department of Energy under Contract # DE-AC02-05CH11231 and Chevron Corporation. The authors are grateful to Dr. Alexander E. Kuperman of Chevron Corporation for the helpful review of the manuscript.

Appendix A. Supplementary material

Supplementary data associated with this article can be found, in the online version, at http://dx.doi.org/10.1016/j.jcat.2012.04.022.

References

[1] G.A. Somorjai, Y. Li, Introduction to Surface Chemistry and Catalysis, second ed., Whiley, 2010.
[2] G.A. Somorjai, J.Y. Park, Angew. Chem., Int. Ed. 47 (2008) 9212.
[3] G.A. Somorjai, A.M. Contreras, M. Montano, R.M. Rioux, Proc. Natl. Acad. Sci. USA 103 (2006) 10577.
[4] K.S. Nagabhushana, H. Bonnemann, Nanotechnol. Catal. 1 (2004) 51.
[5] J.D. Hoefelmeyer, K. Niesz, G.A. Somorjai, T.D. Tilley, Nano Lett. 5 (2005) 435.
[6] H. Song, F. Kim, S. Connor, G.A. Somorjai, P. Yang, J. Phys. Chem. B 109 (2005) 188.
[7] K. Niesz, M. Grass, G.A. Somorjai, Nano Lett. 5 (2005) 2238.
[8] T. Teranishi, M. Hosoe, T. Tanaka, M. Miyake, J. Phys. Chem. B 103 (1999) 3818.
[9] Y. Wang, J. Ren, K. Deng, L. Gui, Y. Tang, Chem. Mater. 12 (2000) 1622.
[10] R.M. Rioux, H. Song, J.D. Hoefelmeyer, P. Yang, G.A. Somorjai, J. Phys. Chem. B 109 (2005) 2192.
[11] H. Lee, S.E. Habas, S. Kweskin, D. Butcher, G.A. Somorjai, P. Yang, Angew. Chem. 118 (2006) 7988.
[12] K. Niesz, M.M. Koebel, G.A. Somorjai, Inorg. Chim. Acta 359 (2006) 2683.
[13] J.Y. Park, Y. Zhang, M. Grass, T. Zhang, G.A. Somorjai, Nano Lett. 8 (2008) 673.
[14] S. Alayoglu, F. Tao, V. Altoe, C. Specht, Z.-W. Zhu, F. Aksoy, D.R. Butcher, R.J. Renzas, Z. Liu, G.A. Somorjai, Catal. Lett. 141 (2011) 633.
[15] M. Boudart, Catal. Support. Met. 2 (1969) 153.
[16] J.M. Basset, G. Dalmai-Imelik, M. Primet, R. Mutin, J. Catal. 37 (1975) 22.
[17] J. Barbier, A. Morales, P. Marecot, R. Maurel, Bull. Soc. Chim. Belg. 88 (1979) 569.
[18] J. Barbier, P. Marecot, Nouveau J. Chim. 5 (1981) 393.
[19] M. Koussathana, D. Vamvouka, H. Economou, X. Verykios, Appl. Catal. 77 (1991) 283.
[20] A.E. Aksoylu, M. Madalena, A. Freitas, M. Fernando, R. Pereira, J.L. Figueiredo, Carbon 39 (2001) 175.
[21] R.V. Hardeveld, F. Hartog, Surf. Sci. 15 (1969) 189.
[22] H. Bonnemann, R.M. Richards, Eur. J. Inorg. Chem. 10 (2001) 2455.
[23] J.N. Kuhn, C.-K. Tsung, W. Huang, G.A. Somorjai, J. Catal. 265 (2009) 209.
[24] J.N. Kuhn, W. Huang, C.K. Tsung, Y. Zhang, G.A. Somorjai, J. Am. Chem. Soc. 130 (2008) 14026.
[25] M.M. Telkar, C.V. Rode, R.V. Chaudhari, S.S. Joshi, A.M. Nalawade, Appl. Catal. A 273 (2004) 11.
[26] A. Quintanilla, V.C.L. Butselaar-Orthlie, C. Kwakernaak, W.G. Sloof, M.T. Kreutzer, F. Kapteijn, J. Catal. 271 (2010).
[27] M.E. Grass, R.M. Rioux, G.A. Somorjai, Catal. Lett. 128 (2009) 1.
[28] Y. Borodko, S.M. Humphrey, T.D. Tilley, H. Frei, G.A. Somorjai, J. Phys. Chem. C 111 (2007) 6288.
[29] Y. Borodko, S.E. Habas, M. Koebel, P. Yang, F. Heinz, G.A. Somorjai, J. Phys. Chem. B 110 (2006) 23052.
[30] P. Antonucci, N. Van Truong, N. Giordano, R. Maggiore, J. Catal. 75 (1982) 140.
[31] J. Le Bars, U. Sprecht, J.S. Bradley, D.G. Blackmond, Langmuir 15 (1999) 7621.
[32] A.F. Flores, R.L. Burwell Jr., J.B. Butt, J. Chem. Soc., Faraday Trans. 88 (1992) 1191.
[33] K.M. Bratlie, L.D. Flores, G.A. Somorjai, J. Phys. Chem. B 110 (2006) 10051.
[34] K.M. Bratlie, C.J. Kliewer, G.A. Somorjai, J. Am. Chem. Soc. 110 (2006) 17925.
[35] K.M. Bratlie, H. Lee, K. Komvopoulos, P. Yang, G.A. Somorjai, Nano Lett. 7 (2007) 3097.
[36] D. Zhao, Q. Huo, J. Feng, B.F. Chmelka, G.D. Stucky, J. Am. Chem. Soc. 120 (1998) 6024.
[37] P. Debye, Ann. Phys. 46 (1915) 809.
[38] M.F.M. Post, A.C. van 't Hoog, J.K. Minderhoud, S.T. Sie, AIChE J. 35 (1989) 1107.
[39] R.J. Madon, M. Boudart, Ind. Eng. Chem. Fundam. 21 (1982) 438.

[40] C.K. Tsung, J.N. Kuhn, W. Huang, C. Aliaga, L.I. Hung, G.A. Somorjai, P. Yang, J. Am. Chem. Soc. 131 (2009) 5816.
[41] G.A. Martin, J.A. Dalmon, J. Catal. 75 (1982) 233.
[42] K.J. Yoon, M.A. Vannice, J. Catal. 82 (1983).
[43] S.D. Lin, M.A. Vannice, J. Catal. 143 (1993) 539.
[44] S.D. Lin, M.A. Vannice, J. Catal. 143 (1993) 563.
[45] S.M. McClure, M. Lundwall, F. Yang, Z. Zhou, D.W. Goodman, J. Phys. Chem. C 113 (2009) 9688.
[46] H. Kubicka, J. Catal. 12 (1968) 223.
[47] G.C. Bond, Appl. Catal. A 191 (2000) 23.